ISSN 1061-8309, Russian Journal of Nondestructive Testing, 2024, Vol. 60, No. 8, pp. 912–920. © Pleiades Publishing, Ltd., 2024.
Russian Text © The Author(s), 2024, published in Defektoskopiya, 2024, No. 8, pp. 42–51.

ELECTROMAGNETIC METHODS

Modeling a Two-Element Tangential Eddy Current Probe with Active Shielding for Soldered Joint Testing

A. E. Gorbunov[a,b,*], P. V. Solomenchuk[b,], and A. S. Umanskii[a,***]**

[a] *St. Petersburg Mining University, St. Petersburg, 199106 Russia*

[b] *Constanta LLC, St. Petersburg, 198098 Russia*

**e-mail: ae.gorbunov.w@gmail.com*

***e-mail: pavel257@mail.ru*

****e-mail: umanskiy_as@pers.spmi.ru*

Received May 21, 2024; revised July 18, 2024; accepted July 19, 2024

Abstract—The paper is devoted to the development of a finite element model of an eddy current probe designed to test the degree of soldering in lap-joint soldered connections of conductive busbars. A methodology for developing a finite element model has been devised that includes a geometric parameter that, when altered, leads to the remeshing of the finite element grid without affecting the test parameters of nondestructive testing. This allows for a series of signal measurements of the finite element model of the eddy current probe, followed by averaging, thereby ensuring acceptable accuracy. The test results confirm the functionality of the eddy current probe, with a defect size measurement range in the soldered joint from 0 to 100% and a guaranteed main absolute error in measuring the degree of soldering of 5%.

Keywords: eddy current testing, solder joint, tangential probe, finite element modeling

DOI: 10.1134/S106183092460196X

INTRODUCTION

When creating a dedicated eddy current probe (ECP) for solving specific problems in the presence of numerous interfering parameters, a lot of resources are spent on developing ECP prototypes. This process is complicated by the lack of the ability to conduct the necessary tests in laboratory conditions. The optimal solution is to develop and verify a virtual model of the ECP and use a physical ECP prototype to confirm the model's characteristics. The paper addresses issues related to designing the virtual model and ensuring the accuracy of signal calculations for the ECP model. The article discusses the process of creating a two-element tangential-type eddy current probe with active shielding designed for inspecting soldered lap joints of stator windings in electric machines (see Fig. 1).

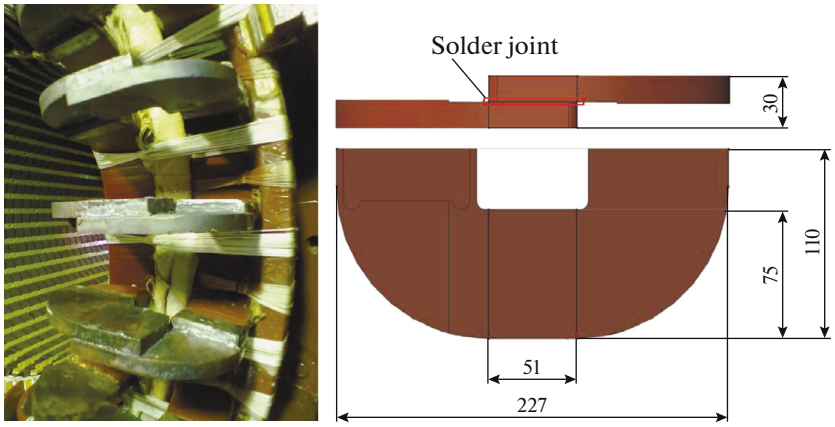


Fig. 1. Soldered connections of copper busbars: photograph (a), sketch (b).

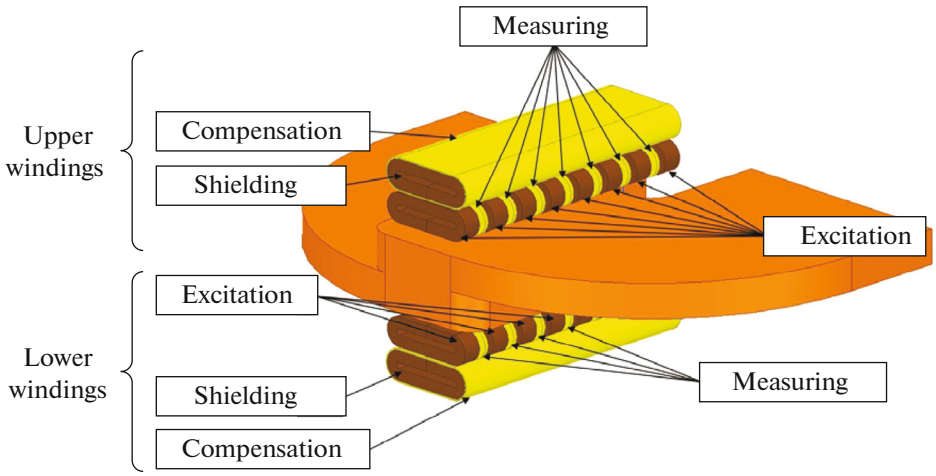


Fig. 2. Close-up of ECP coils and TO.

MODELING EDDY CURRENT PROBES

Several primary methods are used to calculate the parameters of an eddy current probe (ECP): analytical calculations using formulas based on reference literature and modeling using the finite difference method (FDM) and the finite element method (FEM). Analytical calculations of the interaction between the ECP and the test object (TO) yield fairly accurate results [1, 2] but do not account for shielding, material anisotropy, and other specific features [3]. More accurate calculation results are achieved using the FDM and the FEM, which represent the model's elements as a network of points ("nodes") connected in a mesh. In the FDM, calculation results are determined only at the nodes of the mesh, whereas in the FEM, values are computed at every point within the design domain [4]. Consequently, the FDM requires less time and computational resources but provides high accuracy only at the mesh nodes with rough approximation at intermediate points. On the other hand, the FEM ensures high accuracy by integrating over the volume of each finite element (FE) at the cost of increased computational power.

There are many software packages available for solving electromagnetic field modeling problems using FEM. Among them, the most popular programs are ANSYS Maxwell, Altair Flux, COMSOL Multiphysics, JMAG, and SIMULIA Abaqus. In this paper, we used the Ansys Maxwell program, which provides a wide range of possibilities for the operation and optimization of the FE mesh.

FE-Model of ECP for Solder Joint Testing

At the initial stages of creating a model for the interaction between the ECP and the TO using the FEM, the parameters of the model are defined as variables for further optimization or investigation of their impact on the ECP signal when designing a three-dimensional model of the elements (Fig. 2) and the wiring diagram (Fig. 3).

The analyzed ECP consists of two elements placed symmetrically on either side of the TO relative to the plane of the soldered joint. Each element includes four main windings: excitation, measurement, shielding, and compensation ones. A detailed description of the ECP design, the principle of its operation, and the features of the TO can be found in [5–7].

The TO consists of plates made of electrical copper joined in a lap joint with a silver-tin solder to provide electrical contact. The tested area is the surface of the plate junction, and the test parameter is the degree of soldering of the joint expressed as the ratio of the current area of electrical contact between the plates to the plate junction area. The defect simulator is a cold solder in the tested area. A cold solder of the same area affects the signals of the ECP differently in various regions of the tested area. To model the cold solder, its representation is defined as two regions: along the side wall (along the X-axis) and along the end face of the joint (along the Y-axis) (Fig. 4), with their dimensions expressed as a percentage of the soldered joint area.

Several interfering parameters can affect the measurement results in eddy current testing:

1. Parameters of the relative position of the ECP and TO [8, 9].

2. The geometric parameters (shape and dimensions) of the TO [10, 11].

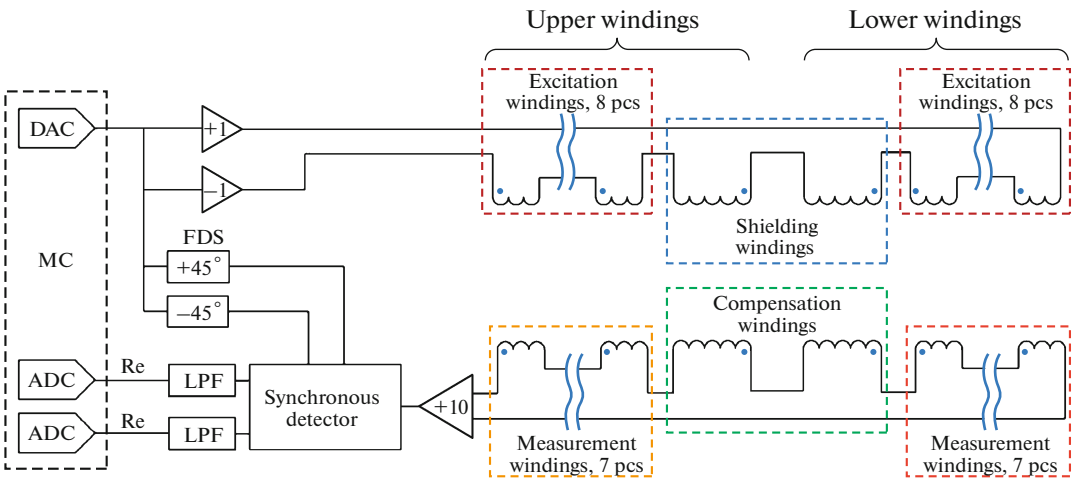


Fig. 3. Wiring diagram of ECP finite-element model.

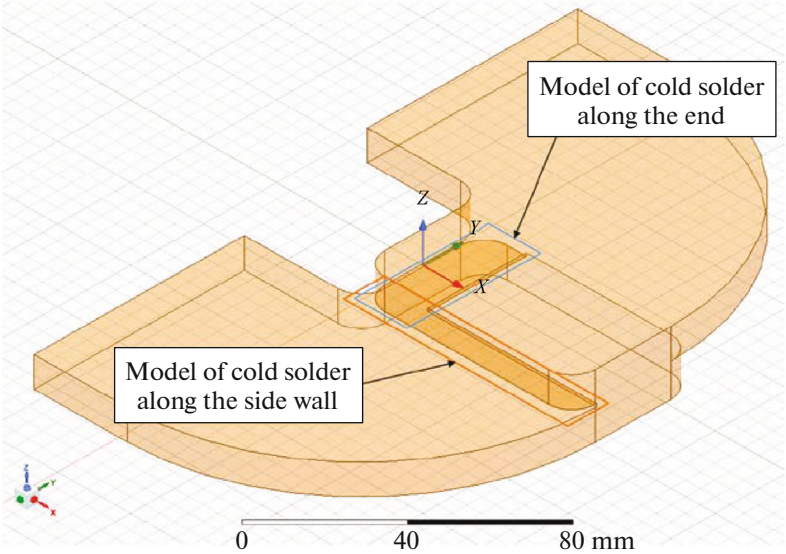


Fig. 4. Models of defect simulators.

3. The electrical parameters (specific electrical conductivity) of the TO [12, 13].

4. Testing conditions (strong magnetic fields or nearby electrically conductive objects).

The following interfering parameters set by variables are investigated in the "ECP–TO" model:

1. The relative position and movement of the ECP and TO along the X-, Y-, and Z-axes.

2. The Distance to adjacent solder joints.

3. The variation in the values of the electrical conductivity of the TO's material.

The ECP signal is the voltage U across the coils of the ECP measuring winding; an informative parameter is its amplitude. The measured value is the soldering degree of the TO expressed in %.

Modeling Accuracy

Ansys Maxwell employs adaptive finite element meshing technology locally adjusting the mesh density of the model based on the gradient data of the analyzed fields until the specified level of energy error or the number of adaptive computations is achieved [15].

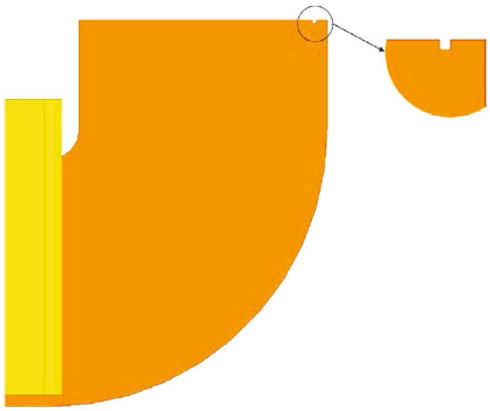


Fig. 5. Cutout in the model.

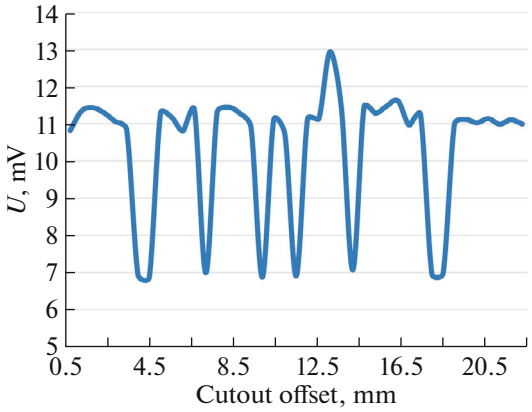


Fig. 6. Dependence of ECP signal on the position of cutout in the model.

The variation in simulation results due to changes in the finite element mesh, while keeping input parameters unchanged, is analyzed by creating a cutout in a remote section of the TO (Fig. 5), the influence of which on the measurement process is negligible [16]. Changing the position of the cutout leads to a rearrangement of the mesh while maintaining other parameters. As a result, a graph of the ECP signal as a function of the cutout position in the model was obtained (Fig. 6). The physical meaning of this graph lies in the variation of the measurement results of the FEM ECP model determined by the reconfiguration of the finite element mesh, and it characterizes the precision of the FEM model. In an ideal FE model, the graph should almost coincide with a straight line.

The precision of the FE model of the ECP is influenced by the following parameters of the FE mesh:

1. Mesh generator choice—classic or tau. The difference between the meshers is that the classic mesher starts by creating a coarse mesh, which is then refined, whereas the tau mesher, on the other hand, begins with a very fine mesh and transitions to a coarser mesh with larger base elements. The classic mesher is better suited for meshing large but thin objects, while the tau generator is more suitable for meshing objects with significant geometric distortions [17].

2. Selecting the number of adaptive passes for the model aimed at improving the accuracy of the model's measurement results. However, increasing the number of algorithm passes does not always improve the precision of the model's signals [18].

3. Limiting the length of the finite element, where the maximum base element size can be specified, thereby forcibly increasing the density of the finite element mesh.

4. Dividing the TO into its component parts. In the model under consideration, the TO is divided into three sections—the tested area and two "tails," each of which can have differently configured mesh parameters.

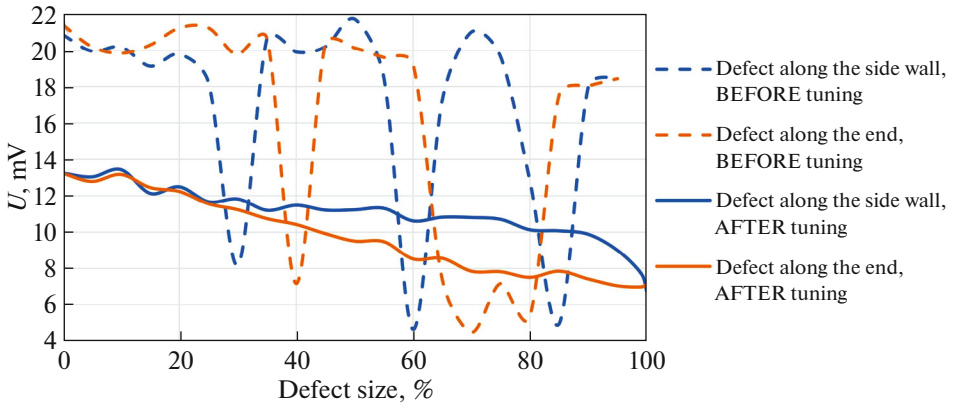


Fig. 7. Comparison of model signals due to two types of cold solder before and after tuning.

5. Building a mesh manually by creating flat or three-dimensional shapes the vertices of which are the mesh nodes.

6. Averaging over 10 values, where a single model signal is calculated as the arithmetic mean of 10 model solutions.

After applying the above-described operations to the model, signals and solution statistics were obtained, the analysis of which allows for selecting optimal settings and parameters for further work with the ECP model. Based on the obtained signals and empirical data, we assume that the amplitude range of the ECP signal when measuring the degree of soldering of the TO is approximately 3 mV, so the signal variation of the ECP model should not exceed 0.5% of this value. The type of distribution of each simulation values is determined using the QQ plot method and the omega-squared method [19].

Thus, only one model meets the set accuracy criteria using the following parameters:

1. Tau mesher.

2. Three passes of adaptive calculation of the FE mesh.

3. Averaging the measurement results of the ECP model over 10 values.

Increasing the required number of solutions by 10 times leads to a rise in time expenditure, although each solution requires relatively few computational resources. Specifically, in our case, the FE model consisted of almost 132000 tetrahedrons, and each solution was completed in 5 min and 14 s, using 2.3 GB of RAM; this allowed for parallel modeling of multiple solutions and achieving an accuracy level of 5%. The quality indicator of the FEM model tuning is the comparison of the ECP defect signals before and after tuning, as shown in Fig. 7, where a considerable improvement in accuracy can be seen.

A high-quality FEM model allows for studying the influence of both the tested and interfering parameters on the ECP signals for further optimization of the design. For this, signals were obtained by varying the following parameters:

1. The controlled parameters:

1.1. The size of the defect located along the TO side wall.

1.2. The size of the defect located along the TO end.

2. The interfering parameters:

2.1. The ECP displacement relative to the TO along the X-, Y-, and Z-axes.

2.2. The change in the specific electrical conductivity of the TO material.

2.3. The change in the distance between adjacent TOs.

As a result, hodograph diagrams of ECP signals describing the influence of these parameters were obtained (Fig. 8).

At this stage, it is important to assess the influence of interfering parameters associated with the ECP location relative to the TO in space. Since the informative parameter of the ECP under consideration is the amplitude of its signal, the complex signal of the interfering parameters related to the ECP position has been recalculated into the amplitude value of the ECP model signal, the dependence graph of which is shown in Fig. 9. The obtained graphs indicate a significant and nonlinear influence of these parameters on the ECP signal, in contrast to the effect of the electrical conductivity of the TO on the signal. At the same time, the impact of technological variations in the thickness of soldered joint components is com-

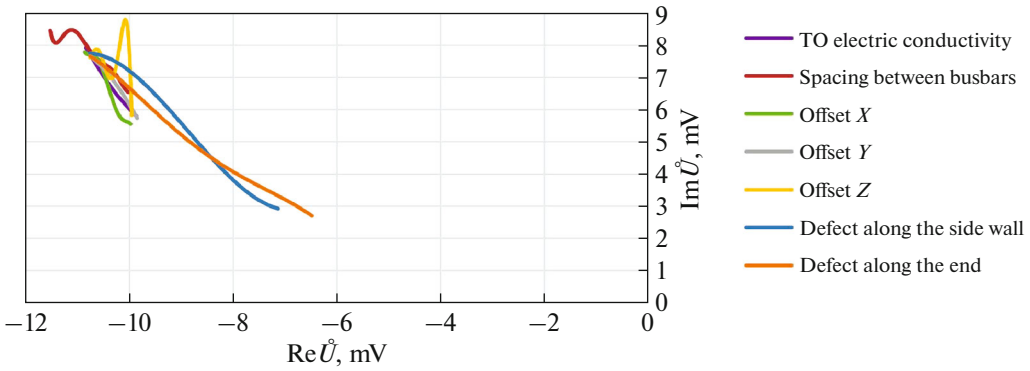


Fig. 8. Hodograph diagrams of defects and interfering parameters.

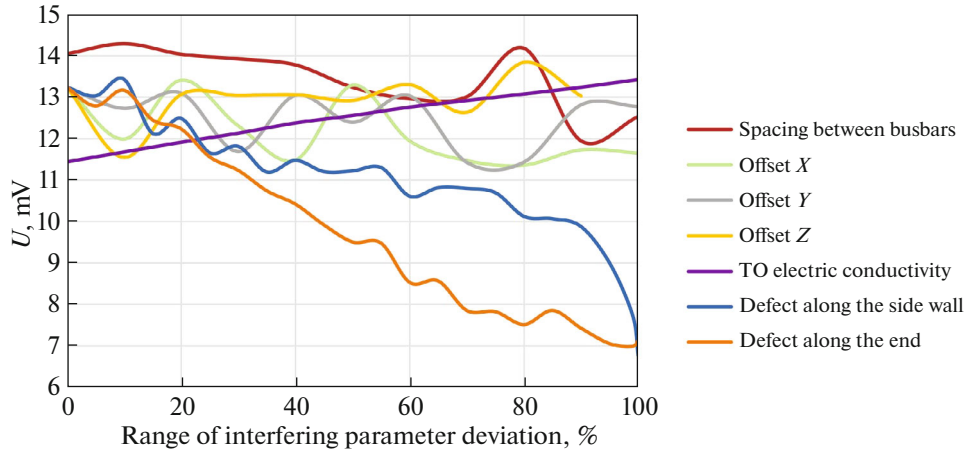


Fig. 9. Influence of test and interfering parameters on the amplitude of ECP signal with the following ranges of interfering parameter deviations: spacing between busbars—from 70 to 90 mm, displacement along the X-axis—from 0 to 10 mm, displacement along the Y-axis—from 0 to 10 mm, displacement along the Z-axis—from 0 to 3 mm, TO electric conductivity—from 40 to 60 mS/m.

parable to the estimated error of the FEM model, making an objective assessment of its influence difficult. The obtained data revealed that effective suppression of the interfering parameters related to the mutual positioning of the ECP and the TO requires means to fix the position of the ECP coils relative to the inspected connection. This was achieved through refinement and optimization of the design.

Based on the model data on the impact of the electrical conductivity of the TO on the ECP signals, a method was developed to mitigate the effect of variations in the electrical conductivity of TO components and control samples on the measurement results of solder joint quality.

TESTING OF THE ECP PROTOTYPE

Based on the ECP simulation results, tooling was created for testing the wire winding technology, balancing the ECP windings, and assessing the influence of certain interfering parameters. For conducting tests, adjusting, and verifying the functionality of the ECP for further operation, calibration samples with 100 and 0% soldering were manufactured. The 100% sample is a solid copper part that replicates the shape and dimensions of the inspected joint, while the 0% sample consists of two solid parts replicating the shape and dimensions of the halves of the inspected joint, glued together with an epoxy adhesive through a fiberglass insulation layer. Additionally, an intermediate 60% sample was made from the 100% sample with a 1 mm wide slot extending 28.8 mm deep across the entire width of the tested zone, simulating

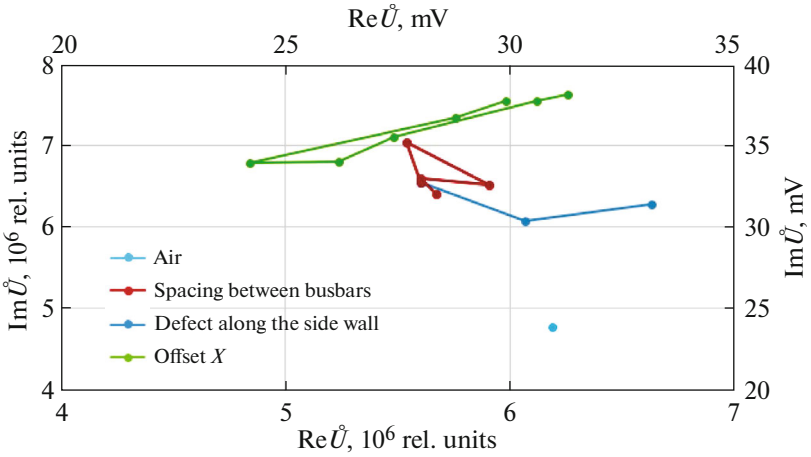


Fig. 10. Test results using balancing equipment.

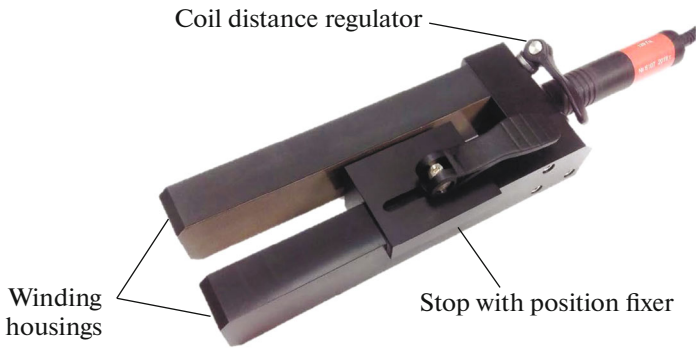


Fig. 11. External ECP view.

a defect along the side wall with an area of 40%. As a result of the tests using the tooling, the hodograph diagrams presented in Fig. 10 were obtained.

Figure 10 shows that the overall character of the ECP signals corresponds to the signals of the ECP model, confirming the sensitivity of the ECP to the expected defects and refining the impact of the interfering parameters. Based on these data, calculations were carried out for the geometry and required stiffness of the ECP components for fixation relative to the TO. The overall view of the finished ECP design is shown in Fig. 11.

The ECP consists of a base to which a handle is attached that contains a board with electronic components. A stationary and a movable plates are fixed to the base, with coils installed inside each of them. The movable plate is secured using a clamp and a backlash-free connection. The plate's movement is sufficient to compensate for the required tolerance of the solder joint thickness across the entire permissible range. On the stationary plate there is a stop fixed to the plate with a clamp designed for positioning the ECP relative to the soldered joint. This stop ensures the consistency of the ECP's positioning relative to the reference piece during calibration and to the soldered joint during inspection.

Multiple measurements were taken on each calibration sample, and the results (Fig. 12) demonstrate a signal-to-noise ratio of 14.7, allowing the precision of the measurements to be assessed.

The test results confirm the ECP's functionality, a defect size measurement range of 0 to 100% for the soldered joint, and compliance with the stated primary absolute measurement error of 5% for soldering quality.

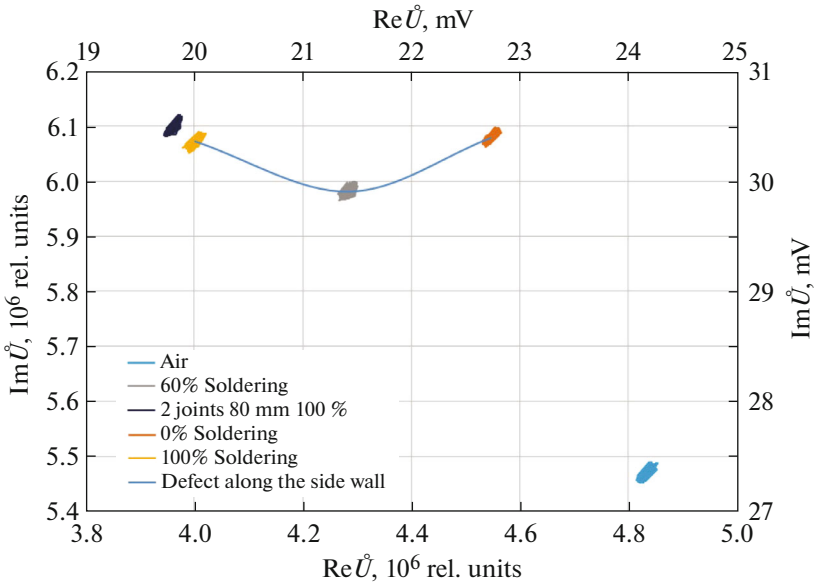


Fig. 12. ECP test results.

CONCLUSIONS

1. A finite element model of the "ECP—TO" has been developed with accuracy parameters that allow for the study of the effects of controlled and interfering parameters on ECP signals for inspecting lap-soldered connections of current-carrying busbars in generator windings.

2. A methodology for designing a finite element model and optimizing parameters has been proposed. This methodology can be used in the development of low-frequency eddy current sensors of various designs and is also applicable to studying the effect of interfering parameters encountered in practice that cannot be reliably reproduced in real test objects or calibration samples.

3. Based on the developed model, an ECP has been created for inspecting lap-soldered connections. This ECP confirms the convergence of measurement results between the finite element model and the actual ECP.

FUNDING

This work was supported by ongoing institutional funding. No additional grants to carry out or direct this particular research were obtained.

CONFLICT OF INTEREST

The authors of this work declare that they have no conflicts of interest.

REFERENCES

1. Syas'ko, V.A. and Chertov, D.N., Detection of delaminations in carbon composite materials using tangential eddy-current sensors, *V Mire NK,* 2012, no. 2, pp. 19–21.
2. Suchkov, G.M. and Khomyak, Yu.V., Improving the capabilities of eddy current testing of the surface of continuously cast slabs of ferromagnetic steels, *Russ. J. Nondestr. Test.,* 2013, no. 1, pp. 78–83.
3. Syas'ko, V.A., Chertov, D.N., and Ivkin, A.E., Measuring the thicknesses of the walls of carbon composite materials using the eddy-current phase method, *Russ. J. Nondestr. Test.,* 2011, vol. 47, pp. 561–567. https://doi.org/10.1134/S1061830911080109
4. Potapov, A.I., Koroteev, M.Yu., Syas'ko, V.A., and Solomenchuk, P.V., A Finite-element modeling of a probe of eddy-current quality testing of soldered joints in turbogenerator windings, *Russ. J. Nondestr. Test.,* 2014, vol. 50, no. 5, pp. 264–273.
5. Gorbunov, A.E., Ivkin, A.E., and Syas'ko, V.A., Patent No. 2808437, *Byull. Izobret.,* 2023, no. 34.

6. Gorbunov, A.E., Ivkin, A.E., and Solomenchuk, P.V., Tangential eddy-current sensor for inspecting lap-welded joints of current-carrying busbars in electrical machines, *Defektoskopiya,* 2023, vol. 11, pp. 54–56. EDN: XBBNOM. https://doi.org/10.31857/S0130308223110052
7. Gorbunov, A.E., Ivkin, A.E., and Solomenchuk, P.V., Measurement of the degree of soldering in the joints of current-carrying busbars of turbo generators using a tangential eddy-current sensor with active shielding, *Phys. Meth. Nondestr. Test. Yanusov Readings Theses XXXIV Ural Conf.* (Ekaterinburg, 2023), pp. 36–37.
8. Kogan, L., Nichipuruk, A., Savary, F., Principe, R., Datskov, V., Rozenfel'd, E., and Khudjakov, B., Eddy current quality of soldered current-carrying bas-bar splices of superconducting magnets, *Insight,* 2015, vol. 57, no. 12, p. 697.
9. Gromyka, D.S. and Gogolinskiy, K.V., Method of state and residual resource assessment of excavator bucket tooth caps, *Russ. J. Nondestr. Test.,* 2022, vol. 58, no. 5, pp. 381–390. https://doi.org/10.1134/S1061830922050035
10. Kogan, L.K., Stashkov, A.N., and Nichiporuk, A.P., Eddy current quality control of soldering in superconducting current-carrying joints with allowance for the effect of cross section variations on testing results, *Russ. J. Nondestr. Test.,* 2019, vol. 55, no. 9, pp. 654–662. https://doi.org/10.1134/S0130308219090033
11. Kogan, L.K., Stashkov, A.N., and Nichiporuk, A.P., Quality control of soldering of side walls of clamps in current-carrying connections of electric machines taking into account the influence of their sizes, *Russ. J. Nondestr. Test.,* 2022, vol. 58, no. 12, pp. 1142–1152. https://doi.org/10.31857/S0130308222120065
12. Kogan, L.Kh., Stashkov, A.N., and Nichipuruk, A.P., Improving the reliability of eddy-current quality control of soldering in current-carrying copper joints and expanding the nomenclature of inspected joints in energy equipment, *Russ. J. Nondestr. Test.,* 2018, vol. 54, no. 11, pp. 784–791.
13. Gonchar, A.V., Klyushnikov, V.A., Mishakin, V.V., and Anosov, M.S., Ultrasonic and eddy-current fatigue monitoring of austenitic steel welded joints, *Russ. J. Nondestr. Test.,* 2021, vol. 57, no. 7, pp. 570–578. https://doi.org/10.1134/S1061830921090126
14. RMG 29-2013. State system for ensuring the uniformity of measurements. Metrology. Basic terms and definitions, 2013.
15. Delphine, D., Pedreira, D., Verbeke, D., Leconte, V., Wendling, P., Loic, R., and Mazauric, V., Adaptive meshing for eddy current calculations, *IEEE Trans. Magnetics,* 2015, vol. 51, no. 11, pp. 1–4. https://doi.org/10.1109/TMAG.2015.2445830
16. Teterko, A.Y., Uchanin, V.M., and Hutnyk, V.I., Improvement of the accuracy of eddy-current testing of the electric conductivity of materials and the thickness of dielectric coatings of the shells, *Mater Sci.,* 2014, vol. 49, pp. 857–865. https://doi.org/10.1007/s11003-014-9684-9
17. Markov, A.A., Mosyagin, V.V., Antipov, A.G., and Ivanov, G.A., The possibility of detecting defects in rail foot by the MFL method, *Russ. J. Nondestr. Test.,* 2024, vol. 60, no. 1, pp. 63–74. https://doi.org/10.1134/S1061830923601459
18. Lehikoinen, A., Arkkio, A., and Belahcen, A., Reduced basis finite element modeling of electrical machines with multiconductor windings, *IEEE Trans. Ind. Appl.,* 2017, vol. 53, no. 5, pp. 4252–4259. https://doi.org/10.1109/ICELMACH.2016.7732918
19. Gogolinskiy, K.V., Ivkin, A.E., Alekhnovich, V.V., Vasil'ev, A.Yu., Tyurnina, A.E., and Vasil'ev, A.S., Assessment of accuracy indicators for coating thickness determination by ball abrasion method, *Zavod. Lab. Diagn. Mater.,* 2020, vol. 86, no. 7, pp. 39–44. https://doi.org/10.26896/1028-6861-2020-86-7-39-44

Publisher's Note. Pleiades Publishing remains neutral with regard to jurisdictional claims in published maps and institutional affiliations.
AI tools may have been used in the translation or editing of this article.